Inorganic Chemistry

Article

Cite This: *Inorg. Chem.* 2019, 58, 6946−6949

pubs.acs.org/IC

Morphology-Directed Synthesis of $LiFePO_4$ and $LiCoPO_4$ from Nanostructured $Li_{1+2x}PO_{3+x}$

Hany El-Shinawi,*[,†] Edmund J. Cussen,[‡,†] and Serena A. Corr*[,†,‡]

[†]Department of Chemical and Biological Engineering, University of Sheffield, Sir Robert Hadfield Building, Sheffield, S1 3JD, U.K.

[‡]Department of Materials Science and Engineering, University of Sheffield, Sir Robert Hadfield Building, Sheffield, S1 3JD, U.K.

Supporting Information

ABSTRACT: A $LiPO_3$-type nanostructure has been developed using a simple microwave approach at temperatures as low as 200 °C. This phase presents an ideal architecture for the morphology-directed synthesis of the olivine-type phases $LiFePO_4$ and $LiCoPO_4$, through a simple and scalable solution-based technique. Pure and carbon-composited olivine phases of interconnected nanoparticulate morphologies display excellent performance at high rates (up to 20 C) over 500 cycles in Li-ion battery cells.

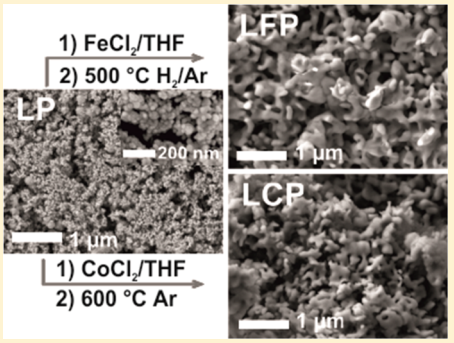

INTRODUCTION

Olivine-type $LiMPO_4$ phases present excellent candidate cathode materials for sustainable and scalable lithium ion (Li-ion) batteries. Their high thermal safety, associated with strong P−O covalent bonding in the olivine structure, their excellent Li-reversibility as demonstrated for phases such as $LiFePO_4$, and their ability to offer a range of operating voltages (e.g., 3.5 and 4.8 V vs Li^+/Li for $LiFePO_4$ and $LiCoPO_4$, respectively) all present considerable advantages.[1,2] While in pristine form the poor intrinsic ionic and electronic conductivities of these materials limit electrochemical performance, this performance can be greatly improved by particle-size reduction, carbon coating, and surface modifications.[3−6] Reducing the particle size of $LiFePO_4$, for example, enables high-rate cycling,[7] attributed to shorter Li-ion path lengths and the formation of a nonequilibrium solid solution phase that inhibits the structural rearrangements typically related to phase transformations during cycling.[8,9] However, nanosizing may adversely affect the tap density and volumetric energy density of electrode materials. To mitigate these effects, porous materials and extended nanostructured architectures have been recently developed through template-assisted and solvothermal syntheses.[10−14] Challenges arise with low-temperature solvothermal methods whereby electrochemical performance can be compromised due to the presence of antisite defects in the crystal structure (i.e., appreciable transition-metal occupancy on the Li sites, leading to blocking the 1D Li-ion pathways in the structure).[15,16] Subsequent postannealing treatments at high temperatures can alleviate this, but typically leads to undesirable particle growth. In this report, we present a new, facile preparation of $LiMPO_4$ and $LiMPO_4/C$ (M = Fe and Co) nanoarchitectures engineered through a morphology-directed synthesis from a nanostructured $LiPO_3$-type precursor. These cathode materials retain porous, extended nanostructured morphologies at temperatures up to 500−600 °C, retaining excellent electrochemical properties.

$LiPO_3$ is conventionally obtained either in a polycrystalline form through high-temperature solid-state reactions or in the form of $50Li_2O−50P_2O_5$ glass.[17] The material crystallizes in a monoclinic unit cell, characterized by infinite linear chains of metaphosphate groups.[18,19] Previously, $LiPO_3$ was reported by Talebi-Esfandarani et al. as a precursor to olivine $LiFePO_4$ by reaction with iron ore concentrates in graphite crucibles at 1100 °C.[20] Such high-temperature treatments can preclude morphology control, resulting in particle growth. Here, we developed a simple approach to synthesize $LiMPO_4$ phases (M = Fe, Co) from lithium-rich $LiPO_3$ at relatively low temperatures, allowing a high degree of control over the final morphology. Nanostructured $LiPO_3$-type material is first obtained via the microwave heat treatment of a tetraglyme solution of phosphorus pentasulfide and lithium *tert*-butoxide at temperatures as low as 200 °C (see Supporting Information for experimental details). This colorless precipitate is subsequently dispersed in a solution containing either $FeCl_2$ or $CoCl_2$, followed by solvent evaporation and a final calcination step at 500−600 °C, to produce nanoarchitectures of $LiFePO_4$ and $LiCoPO_4$.

Received: February 21, 2019
Published: May 8, 2019

DOI: 10.1021/acs.inorgchem.9b00517
Inorg. Chem. 2019, 58, 6946−6949

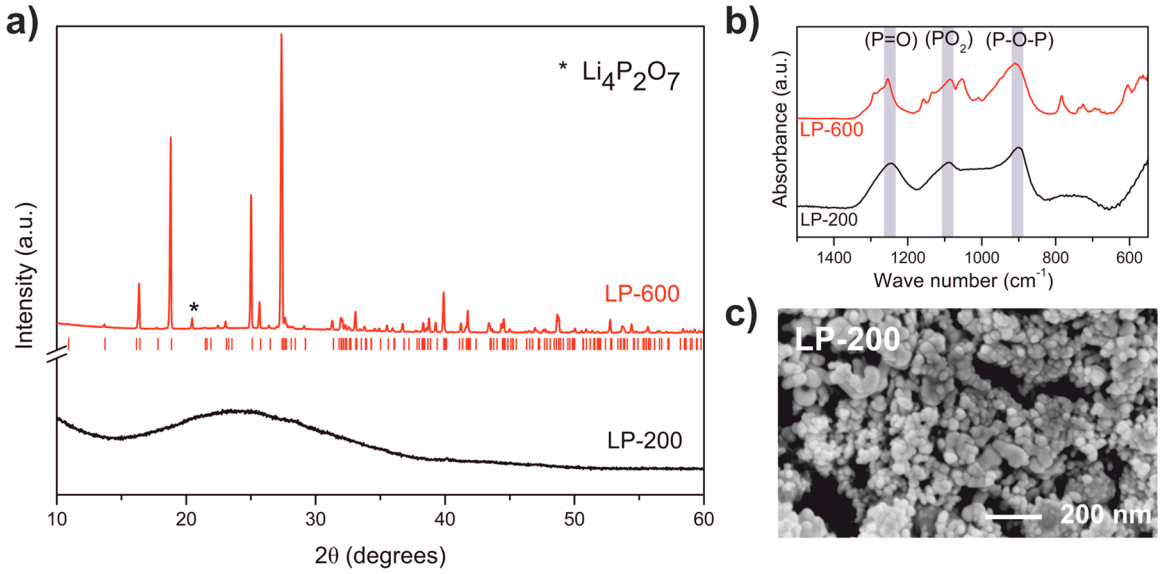

Figure 1. (a) XRD patterns of the $LiPO_3$ phase, synthesized at 200 °C (LP-200, black line) and after calcination at 600 °C (LP-600, red line), with markers shown for crystalline $LiPO_3$.[19] (b) IR spectra of the $LiPO_3$ phase, synthesized at 200 °C (LP-200, black line) and after calcination at 600 °C (LP-600, red line). (c) SEM image of the $LiPO_3$ phase synthesized at 200 °C.

RESULTS AND DISCUSSION

The as-synthesized $LiPO_3$ has been characterized by X-ray powder diffraction (XRD), induced coupled plasma mass spectroscopy (ICP-MS), Fourier transform infrared spectroscopy (FTIR), and scanning electron microscopy (SEM). Elemental analysis showed no evidence for the presence of sulfur and reveals a Li:P molar ratio of 1.21(8):1. XRD analysis indicates that an amorphous material is obtained. On heating this sample to 600 °C, a characteristic XRD pattern of crystalline $LiPO_3$ is found (Figure 1a), suggesting the as-synthesized material is likely an amorphous $LiPO_3$-type phase. The appearance of a small impurity of Li-rich $Li_4P_2O_7$ in the XRD pattern after calcination at 600 °C (Figure 1a) is consistent with the ICP-MS analysis, indicating a lithium-rich material (i.e., $Li_{1+2x}PO_{3+x}$). Figure 1b shows IR spectra for the as-synthesized material and the material calcined at 600 °C, both displaying characteristic peaks corresponding to vibrational modes of the PO_4 tetrahedra and the P−O−P bonds present in $LiPO_3$ phosphate chains.[21−23] Interestingly, SEM images reveal a novel nanoparticulate morphology (Figure 1c), with typical particle sizes ranging from 20 to 35 nm (see Figure S1). The material showed a large specific surface area of 41.6 $m^2\ g^{-1}$, as determined from nitrogen adsorption using the Brunauer−Emmett−Teller (BET) method. To investigate the potential for this X-ray amorphous and high-surface-area material as a precursor for the synthesis of olivine $LiMPO_4$ compounds under mild conditions, the as-synthesized $LiPO_3$ was immersed in suitable metal ion solutions followed by solvent evaporation and calcination. $LiFePO_4$ and $LiCoPO_4$ were successfully synthesized using this approach, where $LiPO_3$ is dispersed in tetrahydrofuran (THF) solutions of $FeCl_2$ and $CoCl_2$, followed by a calcination step after solvent evaporation at 500−600 °C under either inert (Ar) or reducing (H_2/Ar) atmospheres (Figure 2a). Thanks to the relatively low calcination temperature, this approach offers excellent control over the resulting morphology, inhibiting large particle growth. SEM analyses of the obtained $LiMPO_4$ phases reveal networks of interconnected nanoparticles with open pores enabling shorter path lengths for Li-ion transport and large electrode−

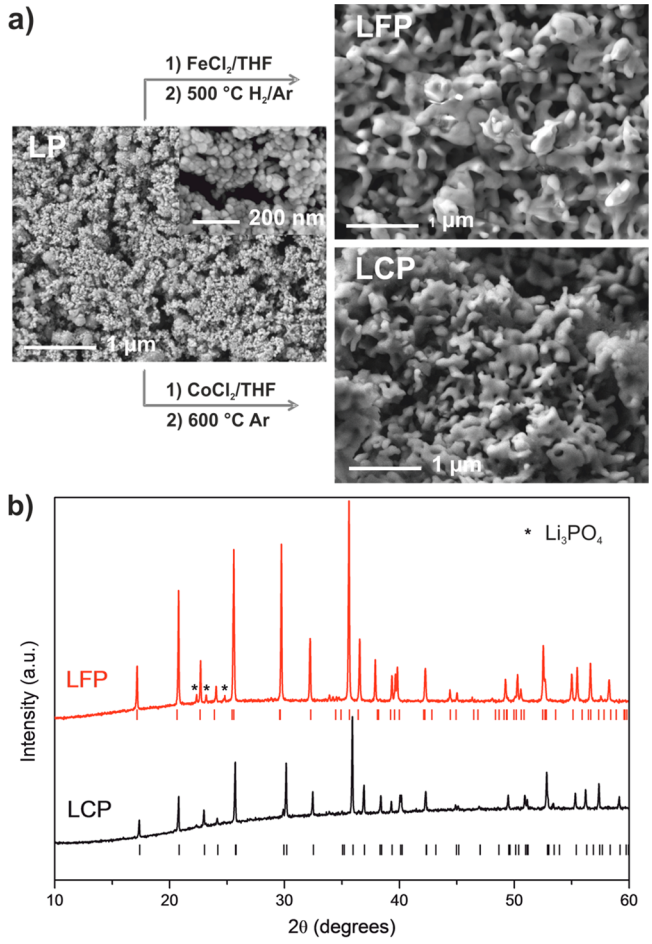

Figure 2. (a) Morphologies of the as-synthesized $LiPO_3$ phase (LP), $LiFePO_4$ (LFP), and $LiCoPO_4$ (LCP). (b) XRD patterns of $LiFePO_4$ (LFP) and $LiCoPO_4$ (LCP). The top markers (red) are for $LiFePO_4$, and the bottom markers (black) are for $LiCoPO_4$.

electrolyte contact areas (Figure 2a).[10−14] BET surface analysis revealed specific surface areas of 18.1 and 12.6 $m^2\ g^{-1}$ for

DOI: 10.1021/acs.inorgchem.9b00517
Inorg. Chem. 2019, 58, 6946−6949

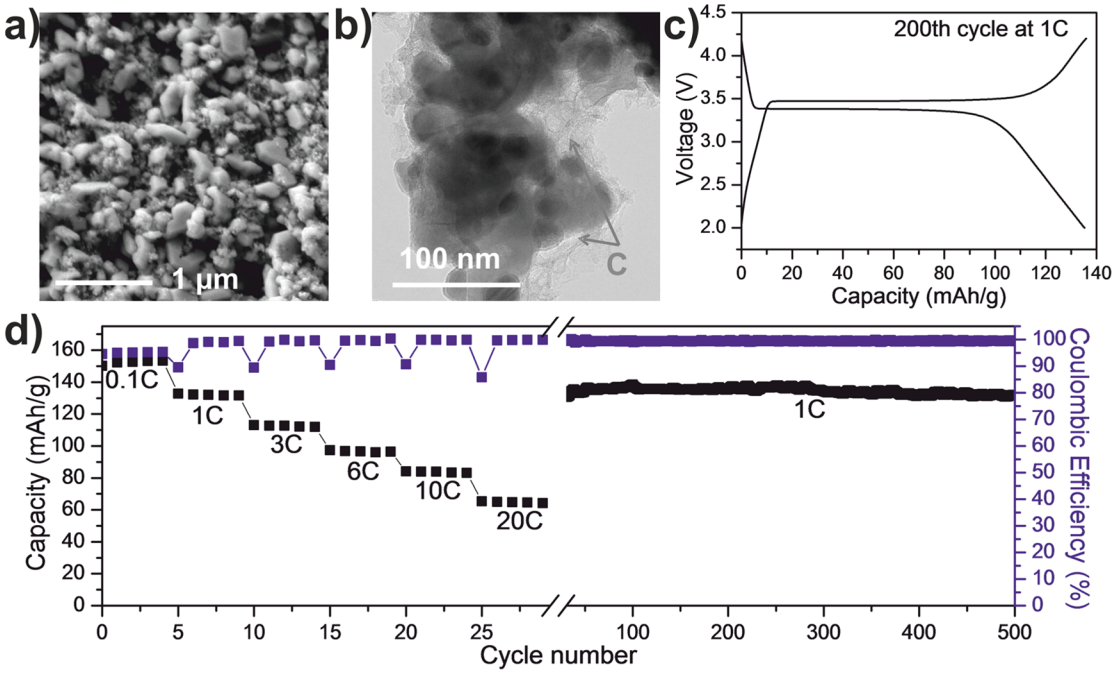

Figure 3. (a) SEM and (b) TEM images of the $LiFePO_4$/C composite. (c) Representative charge/discharge profile of the $LiFePO_4$/C composite, represented by the 200th cycle at 1C rate (1C corresponds to 170 mA g^{-1}). (d) Specific capacity as a function of cycle number for $LiFePO_4$/C at different charge−discharge rates.

$LiFePO_4$ and $LiCoPO_4$, respectively. Samples of $LiFePO_4$ and $LiCoPO_4$ were annealed in air at 550 °C to ensure removal of carbon prior to surface area measurements. Figure 2b shows XRD data collected from the synthesized materials.

A small amount of Li_3PO_4 (5.0(5) wt %; see Figure S2) is observed in the case of $LiFePO_4$, while $LiCoPO_4$ is obtained predominately as a single phase. Refined data, against olivine-type structure with orthorhombic unit cells (Figure S2), reveal unit cell parameters of a = 10.3306(1) Å, b = 6.0089(1) Å, c = 4.69415(8) Å and a = 10.2044(2) Å, b = 5.9208(1) Å, c = 4.6994(1) Å for $LiFePO_4$ and $LiCoPO_4$, respectively, consistent with previous reports.[24,25] ICP-MS analysis indicated M:Li ratios of 1:0.98(3) and 1:1.13(3) for $LiCoPO_4$ and $LiFePO_4$, respectively, consistent with the presence of a small Li_3PO_4 impurity for $LiFePO_4$.

In addition to providing a simple route to controlled $LiMPO_4$ particle morphology, we demonstrate that the same approach can be modified to obtain $LiMPO_4$/C composite phases where this nanostructured morphology is retained. $FeCl_2$ and $CoCl_2$ form relatively stable complexes with the THF solvent,[26] thus enabling the formation of $LiPO_3/MCl_2$/THF solid precursors through slow evaporation of excess THF at ∼70−80 °C. These solid precursors are directly converted to $LiMPO_4$/C nanocomposites after calcination in an oxygen-free atmosphere. Carbon-free materials are achieved through removal of THF from the $LiPO_3/MCl_2$/THF solid precursors by precalcination in air at suitable temperature (∼300 °C) prior to a final calcination step under inert conditions.

Interestingly, the $LiFePO_4$/C composite retains its interconnected nanoparticulate morphology, with carbon homogeneously surrounding the nanoparticles (Figure 3 and Figure S3). Elemental analysis indicates a carbon content of 2.8 wt %. Figure 3c displays a typical discharge/charge profile of the $LiFePO_4$/C composite at room temperature at a 1C rate, represented by the 200th cycle (Li metal anode; 1 M $LiPF_6$ in 1:1 EC/DMC). A specific capacity of 153 mAh g^{-1} is observed at 0.1C rate, with capacities of up to 65 mAh g^{-1} at 20C rate. The material also shows an excellent cyclability, retaining a capacity of 130 mAh g^{-1} after 500 cycles at 1C rate. The excellent electrochemical performance suggests this synthetic approach affords materials with a lack of defects that can inhibit Li-ion diffusion. This is consistent with FTIR observations of the $LiFePO_4$ and $LiFePO_4$/C phases (see Figure S4), where the P−O vibration of the PO_4 groups at 959 cm^{-1} is very close to the value expected for defect-free $LiFePO_4$ (957 cm^{-1}), assuming sensitivity of this vibration mode to anti-site defect formation.[16]

CONCLUSION

The synthetic approach developed here presents a new route to $LiMPO_4$ electrode materials through a soft chemical route that maintains the parent $LiPO_3$ nanostructured morphology. The development of nanostructured $LiPO_3$ as a precursor material opens up the possibility of chemically tuning the metal content in $LiMPO_4$ in nanoparticulate forms with high surface areas. The development of this simple and scalable route to nanostructured $LiPO_3$ provides an alternative to conventional polycrystalline and glass forms, often synthesized at temperatures exceeding 550 °C. This morphology-directed approach to electrode nanoarchitectures also demonstrates great promise for obtaining carbon-composited olivines with excellent battery performance and cycling stability up to 500 cycles.

ASSOCIATED CONTENT

Supporting Information

The Supporting Information is available free of charge on the ACS Publications website at DOI: 10.1021/acs.inorgchem.9b00517.

DOI: 10.1021/acs.inorgchem.9b00517
Inorg. Chem. 2019, 58, 6946−6949

Further details of experimental procedures, Rietveld refinements and diffraction patterns, and FTIR spectra (PDF)

AUTHOR INFORMATION

Corresponding Authors

*E-mail: h.z.el-shinawi@sheffield.ac.uk.
*E-mail: s.corr@sheffield.ac.uk.

ORCID

Hany El-Shinawi: 0000-0002-4743-5576
Serena A. Corr: 0000-0002-9303-4220

Author Contributions

All authors have given approval to the final version of the manuscript.

Funding

This work was supported by funding from the EPSRC (EP/N001982/1), and we thank the Departments of Chemical and Biological Engineering and Materials Science and Engineering at the University of Sheffield for their support of our research.

Notes

The authors declare no competing financial interest.

ACKNOWLEDGMENTS

The authors gratefully acknowledge the wonderful expertise, help, and technical support of Mr. Michael Beglan at the School of Chemistry, University of Glasgow. We thank Mr. Peter Chung (School of Geographical and Earth Sciences, University of Glasgow) for his valuable assistance with SEM and EDS measurements and Mr. Colin How (School of Physics and Astronomy, University of Glasgow) for collecting TEM images.

REFERENCES

(1) Padhi, A. K.; Nanjundaswamy, K. S.; Goodenough, J. B. Phospho olivines as Positive Electrode Materials for Rechargeable Lithium Batteries. *J. Electrochem. Soc.* **1997**, *144*, 1188−1194.

(2) Amine, K.; Yasuda, H.; Yamachi, M. Olivine $LiCoPO_4$ as 4.8 V Electrode Material for Lithium Batteries. *Electrochem. Solid-State Lett.* **1999**, *3*, 178−179.

(3) Yuan, L. X.; Wang, Z. H.; Zhang, W. X.; Hu, X. L.; Chen, J. T.; Huang, Y. H.; Goodenough, J. B. Development and challenges of $LiFePO_4$ cathode material for lithium-ion batteries. *Energy Environ. Sci.* **2011**, *4*, 269−284.

(4) Wang, J.; Sun, X. Understanding and recent development of carbon coating on $LiFePO_4$ cathode materials for lithium-ion batteries. *Energy Environ. Sci.* **2012**, *5*, 5163−518.

(5) Wang, J.; Sun, X. Olivine $LiFePO_4$: the remaining challenges for future energy storage. *Energy Environ. Sci.* **2015**, *8*, 1110−1138.

(6) Zhang, M.; Garcia-Araez, N.; Hector, A. L. Understanding and development of olivine $LiCoPO_4$ cathode materials for lithium-ion batteries. *J. Mater. Chem. A* **2018**, *6*, 14483−14517.

(7) Kang, B.; Ceder, G. Battery materials for ultrafast charging and discharging. *Nature* **2009**, *458*, 190−193.

(8) Malik, R.; Zhou, F.; Ceder, G. Kinetics of non-equilibrium lithium incorporation in LiFePO4. *Nat. Mater.* **2011**, *10*, 587−590.

(9) Liu, H.; Strobridge, F. C.; Borkiewicz, O. J.; Wiaderek, K. M.; Chapman, K. W.; Chupas, P. J.; Grey, C. P. Capturing metastable structures during high-rate cycling of $LiFePO_4$ nanoparticle electrodes. *Science* **2014**, *344*, 1252817.

(10) Hill, M. R.; Wilson, G. J.; Bourgeois, L.; Pandolfo, A. G. High Surface Area Templated $LiFePO_4$ from a Single Source Precursor Molecule Energy. *Energy Environ. Sci.* **2011**, *4*, 965−972.

(11) Fischer, M. G.; Hua, X.; Wilts, B. D.; Castillo-Martínez, E.; Steiner, U. Polymer-Templated $LiFePO_4$/C Nanonetworks as High-Performance Cathode Materials for Lithium-Ion Batteries. *ACS Appl. Mater. Interfaces* **2018**, *10* (2), 1646−1653.

(12) Sun, C.; Rajasekhara, S.; Goodenough, J. B.; Zhou, F. Monodisperse Porous $LiFePO_4$ Microspheres for a High Power Li-Ion Battery Cathode. *J. Am. Chem. Soc.* **2011**, *133*, 2132−2135.

(13) Zhang, Q.; Huang, S.-Z.; Jin, J.; Liu, J.; Li, Y.; Wang, H.-E.; Chen, L.-H.; Wang, B.-J.; Su, B.-L. Engineering 3D bicontinuous hierarchically macro-mesoporous $LiFePO_4$/C nanocomposite for lithium storage with high rate capability and long cycle stability. *Sci. Rep.* **2016**, *6*, 25942.

(14) Liu, Y.; Gu, J.; Zhang, J.; Yu, F.; Dong, L.; Nie, N.; Li, W. Metal organic frameworks derived porous lithium iron phosphate with continuous nitrogen-doped carbon networks for lithium ion batteries. *J. Power Sources* **2016**, *304*, 42.

(15) Jensen, K. M. Ø.; Christensen, M.; Gunnlaugsson, H. P.; Lock, N.; Bøjesen, E. D.; Proffen, T.; Iversen, B. B. Defects in Hydrothermally Synthesized $LiFePO_4$ and $LiFe_{1-x}Mn_xPO_4$ Cathode Materials. *Chem. Mater.* **2013**, *25* (11), 2282−2290.

(16) Qin, X.; Wang, J.; Xie, J.; Li, F.; Wen, L.; Wang, X. Hydrothermally synthesized $LiFePO_4$ crystals with enhanced electrochemical properties: simultaneous suppression of crystal growth along [010] and anti-site defect formation. *Phys. Chem. Chem. Phys.* **2012**, *14*, 2669−2677.

(17) Money, B. K.; Hariharan, K. Lithium ion conduction in lithium metaphosphate based systems. *Appl. Phys. A: Mater. Sci. Process.* **2007**, *88*, 647−652.

(18) Guitel, J. C.; Tordjman, I. Structure Cristalline du Polyphosphate de Lithium, $LiPO_3$. *Acta Crystallogr., Sect. B: Struct. Crystallogr. Cryst. Chem.* **1976**, *32*, 2960.

(19) Murashova, E. V.; Chudinova, N. N. Synthesis and crystal structures of lithium polyphosphates, $LiPO_3$, $Li_4H(PO_3)_5$, and $LiMn(PO_3)_3$. *Crystallogr. Rep.* **2001**, *46*, 942.

(20) Talebi-Esfandarani, M.; Rousselot, S.; Gauthier, M.; Sauriol, P.; Liang, G.; Dollé, M. $LiFePO_4$ synthesized via melt synthesis using low-cost iron precursors. *J. Solid State Electrochem.* **2016**, *20*, 1821−1829.

(21) Moreau, F.; Durán, A.; Muñoz, F. Structure and properties of high Li_2O-containing aluminophosphate glasses. *J. Eur. Ceram. Soc.* **2009**, *29*, 1895.

(22) Pershina, S. V.; Raskovalov, A. A.; Antonov, B. D.; Reznitskikh, O. G.; Vovkotrub, E. G.; Batalov, N. N.; Kadyrova, N. I. Structure and properties of $(1-x)LiPO_{3-x}$ SiO_2 and $50Li_2O$-$(50-x)P_2O_{5-x}$ SiO_2 glass-forming systems. *Russ. J. Phys. Chem.* **2016**, *90*, 2194.

(23) Pershina, S. V.; Raskovalov, A. A.; Antonov, B. D.; Yaroslavtseva, T. V.; Reznitskikh, O. G.; Baklanova, Y. V.; Pletneva, E. D. Extreme behavior of Li-ion conductivity in the $Li_2O-Al_2O_3-P_2O_5$ glass system. *J. Non-Cryst. Solids* **2015**, *430*, 64.

(24) Streltsov, V. A.; Belokoneva, E. L.; Tsirelson, V. G.; Hansen, N. K. Multipole analysis of the electron density in triphylite, $LiFePO_4$, using X-ray diffraction data. *Acta Crystallogr., Sect. B: Struct. Sci.* **1993**, *49*, 147−153.

(25) Kubel, F. Crystal structure of lithium cobalt double orthophosphate, $LiCoPO_4$ Z. Kristallogr. *Z. Kristallogr. - Cryst. Mater.* **1994**, *209*, 755−755.

(26) Kern, R. J. Tetrahydrofuran complexes of transition metal chlorides. *J. Inorg. Nucl. Chem.* **1962**, *24*, 1105−1109.

DOI: 10.1021/acs.inorgchem.9b00517
Inorg. Chem. 2019, 58, 6946−6949